Paleomagnetic and geochronological study of the Halaqiaola basalts, southern margin of the Altai Mountains, northern Xinjiang: Constraints on neotectonic convergent patterns north of Tibet

Baochun Huang

Paleomagnetism and Geochronology Laboratory of the State Key Laboratory of Lithosphere Evolution, Institute of Geology and Geophysics, Chinese Academy of Sciences, Beijing, China

John D. A. Piper

Geomagnetism Laboratory, Department of Earth and Ocean Sciences, University of Liverpool, Liverpool, UK

Huaiyu He, Chunxia Zhang, and Rixiang Zhu

Paleomagnetism and Geochronology Laboratory of the State Key Laboratory of Lithosphere Evolution, Institute of Geology and Geophysics, Chinese Academy of Sciences, Beijing, China

Received 16 June 2005; revised 3 October 2005; accepted 25 October 2005; published 13 January 2006.

[1] A combined geochronological and paleomagnetic study is reported from Miocene basalts from Halaqiaola and Paleocene to Eocene red beds from Fuyun at the southern Altai Mountains, northern Xinjiang. Three new $^{40}Ar/^{39}Ar$ ages determined by fresh matrix from the Halaqiaola basalts collectively confirm the presence of Cenozoic magmatic activity in the northern Xinjiang. Alternating field and thermal demagnetization identify stable characteristic remanences with single reversed polarity in the basalts and red beds. Rock magnetic analysis identifies pseudosingle-domain titanomagnetites as carriers of remanence in the basalts. Paleomagnetic results from the Fuyun red beds indicate that inclination shallowing is present in this rock facies as also found in previous red bed studies from central Asia. In contrast, the time-averaged paleomagnetic direction from the basalts shows that no paleomagnetically discernible northward convergence has occurred north of Junggar since early Miocene times. Analysis of available Cretaceous and Cenozoic paleomagnetic data from volcanic rocks in central Asia shows that Neogene and Quaternary paleolatitudes are statistically concordant with predicted values from Eurasian references, suggesting that no significant northward convergence has occurred north of Tibet during the last 20 Myr. Cretaceous and Paleogene paleolatitudes lie $\sim 5-6 \pm 7^{\circ}$ south of predicted values from the Eurasian path and suggest that neotectonic convergence of the order of several hundred kilometers has occurred north of the southwest Tian Shan. It is possible that neotectonic northward convergence north of Tibet will prove to be paleomagnetically undetectable, but more data are required to confirm this.

Citation: Huang, B., J. D. A. Piper, H. He, C. Zhang, and R. Zhu (2006), Paleomagnetic and geochronological study of the Halaqiaola basalts, southern margin of the Altai Mountains, northern Xinjiang: Constraints on neotectonic convergent patterns north of Tibet, *J. Geophys. Res.*, *111*, B01101, doi:10.1029/2005JB003890.

1. Introduction

[2] Distributed and differential crustal deformation in the major mountain ranges between India and Siberia, including the Himalaya, Kunlun, Tian Shan, and Altai (Figure 1a), has resulted from the ongoing impingement of India into Asia during the past 50 Myr [e.g., *Patriat and Achache*, 1984] and has been evaluated by a wide range of geological and geophysical investigations [e.g., *Molnar and Tapponnier*, 1975; *Patriat and Achache*, 1984; *Achache and Courtillot*, 1984; *Besse et al.*, 1984; *Dewey et al.*, 1988; *Chen et al.*, 1991, 1992; *Le Pichon et al.*, 1992; *Meyer et al.*, 1998; *Yin and Harrison*, 2000; *Tapponnier et al.*, 2001]. This neotectonic (postcollisional) deformation has mostly been characterized by intracontinental shortening and lithosphere thickening in Tibet and central Asia, and the dramatic crustal shortening in Tibet and areas to the north has been recognized by a range of geophysical data [*Patriat and Achache*, 1984; *Achache and Courtillot*, 1984; *Besse et al.*, 1984; *Chen et al.*, 1991, 1992, 1993] and by volumetric analysis [*Le Pichon et al.*, 1992]. These studies suggest that

0148-0227/06/2005JB003890$09.00

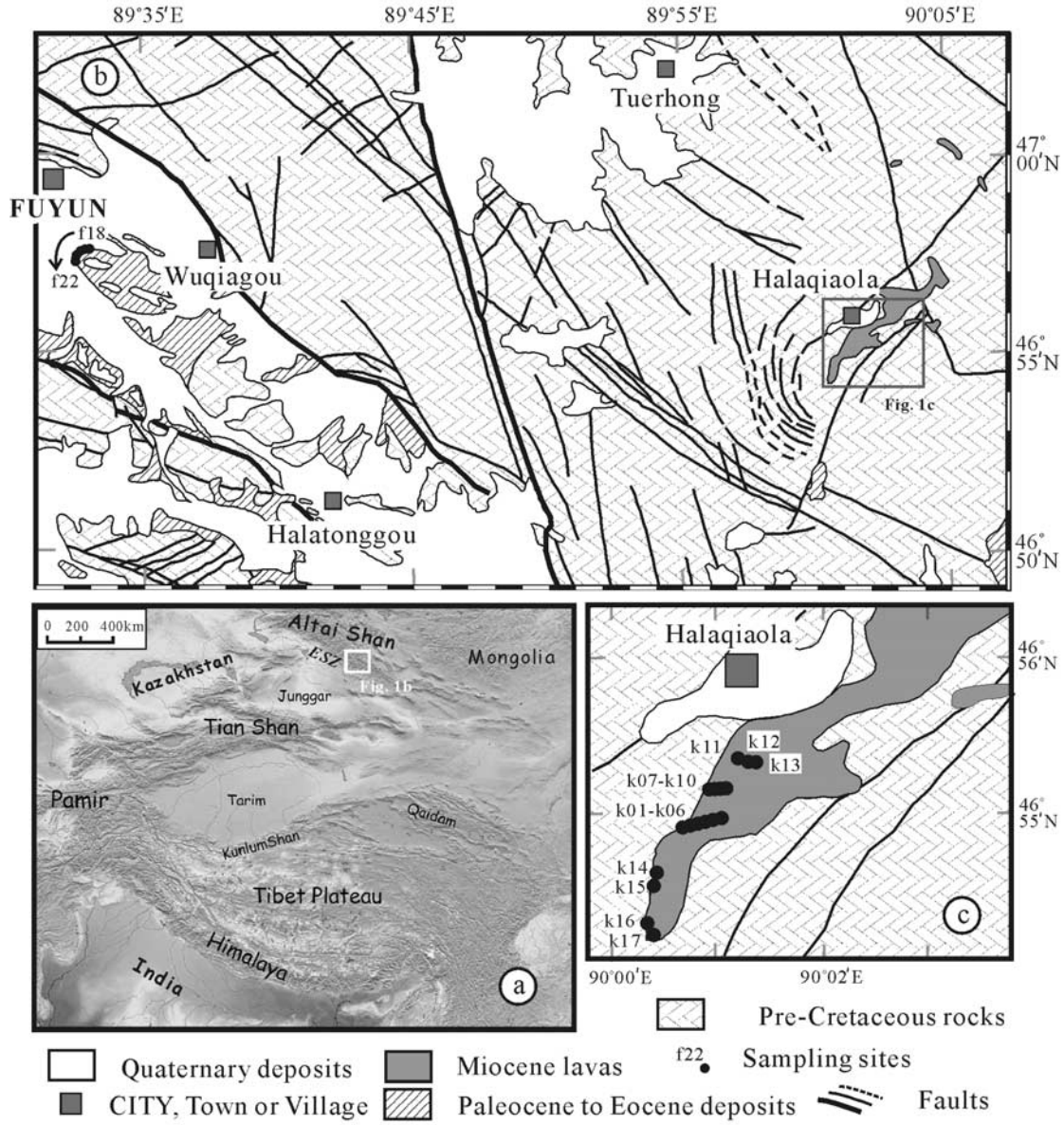

Figure 1. (a) Topographic map of Tibet and central Asia showing the tectonic framework and geotectonic units. The Erqisi Suture Zone (ESZ) is considered to be the last suture to weld the Siberian Plate with the Junggar Block of the Kazakhstan-Junggar Plate [e.g., *Xiao et al.*, 1992]. (b) Simplified regional geological map of Fuyun County and adjacent areas showing post-Cretaceous stratigraphy and areas sampled for this study. Redrawn from regional geological maps of Fuyun and Qinghe counties, scale 1:200000 [*TRGSX*, 1978a, 1978b]. (c) Geological sketch of the area near Halaqiaola Village showing the distribution of sampling sites.

overall convergence between India and Siberia since onset of collision has been some 2700 km, of which ~1500 km has occurred north of Tibet. However, a deficit of the order of 1000 km comes from direct comparison between this overall convergence and an expanding range of geological observations in Tibet and areas to the north [e.g., *Dewey et al.*, 1988, 1989; *Avouac et al.*, 1993; *Murphy et al.*, 1997; *Yin and Harrison*, 2000; *Johnson*, 2002, and references therein].

[3] Paleomagnetic results from the lower and upper basalt series in the Tuoyun Basin of the southwest Tian Shan [*Gilder et al.*, 2003; *Huang et al.*, 2005] are concordant at the 95% confidence level, and both studies indicate that little or no neotectonic northward convergence has taken place in the southwest Tian Shan. This evidence together with other recent paleomagnetic data from volcanic rocks in central Asia [e.g., *Otofuji et al.*, 1995; *Li et al.*, 1995; *Meng et al.*, 1998; *Bazhenov and Mikolaichuk*, 2002; *Gilder et al.*, 2003], has led us to propose that neotectonic northward convergence north of Tarim was evidently less than 1000 km, and that earlier overestimation of the total amount of neotectonic northward convergence north of Tibet is probably responsible for the apparent shortening deficit in Tibet and its hinterland [*Huang et al.*, 2005].

[4] In the eastern part of Tibet and areas to the north it has been proposed that northward convergence of some 600 km has been absorbed in the northernmost Altai Mountains (also known as Altai Shan, Figure 1a) since onset of the India/Asia collision [*Chen et al.*, 1991]. However, GPS vectors from the southern margin of the Altai Mountains show virtually no present-day crustal deformation of that area with respect to Eurasia [*Wang et al.*, 2001]. Repeated paleomagnetic data sets in central Asian Cretaceous and Tertiary red beds show a strong bias toward shallow inclinations [e.g., *Thomas et al.*, 1993; *Chauvin et al.*, 1996; *Gilder et al.*, 2001, 2003; *Cogné et al.*, 1999; *Dupont-Nivet et al.*, 2002; *Huang et al.*, 2004] and are probably unreliable indicators for the long-term effects of crustal shortening because these inclinations could plausibly be attributed to sedimentary inclination shallowing [*Tan et al.*, 2003; *Tauxe*, 2005]. However, there are still no paleomagnetic data from volcanic rocks in the northern part of Xinjiang lying north to the Tian Shan Range that could be more reliably used to investigate neotectonic convergence in this northernmost zone of compressive strain linked to Himalayan deformation. This shortfall comes from a traditional view that no Cenozoic magmatic activity occurred in the northern part of Xinjiang north to the Tian Shan Range [e.g., *Xingjiang Regional Stratigraphic Tables Compilation Team* (XRSCT), 1981].

[5] This traditional view was changed by $^{40}Ar/^{39}Ar$ study of the Halaqiaola basalts [*Zhang et al.*, 1994] in the region to the east of Fuyun city at the southern margin of the Altai Mountains (Figure 1b), which were formerly thought to be of Jurassic age [*Team of Regional Geological Survey of Xinjiang Uygur Autonomous Region* (TRGSX), 1978a; *XRSCT*, 1981]. In this paper we report paleomagnetic study and a further geochronological investigation of these basalts. Concordant $^{40}Ar/^{39}Ar$ ages of some 17 Ma for three discrete flows in the Halaqiaola basaltic succession provide powerful constraints on the timing of magmatic activity and paleomagnetic investigation of 17 sites collected from at least five discrete flows allows us to evaluate the northward convergence pattern in the Altai Mountains since early Miocene times. Together with an updated assessment of Cretaceous and Cenozoic paleomagnetic results from volcanic rocks in the central Asian terranes, these results permit a first-order evaluation of the northward convergence that has occurred north of Tibet since onset of the India/Asia collision. We have in addition, sampled some Paleocene to Eocene red beds from a region ~50 km west of the Halaqiaola basalt outcrop flows and find that paleomagnetic directions recorded in red beds from the southern margin of the Altai Mountains show significant bias toward shallow paleomagnetic inclinations.

2. Geological Framework and Sampling

[6] The Altai Mountains record the northernmost zone of major neotectonic deformation resulting from compressive strain imparted by Himalayan collision in the region of Tibet and central Asia. This range has a NW-SE orientation from Kazakhstan in the west to western Mongolia in the east and extends from Russia to the northern region of Xinjiang, China (Figure 1a). The mountain range links the Kazakhstan–Junggar Plate to the south with the Siberian Plate to the north and is a component of the huge Paleozoic central Asian orogenic belt interpreted as originating at a southwest subduction–accreted continental margin of the Siberian Plate during Paleozoic times [e.g., *Şengor et al.*, 1993]. On the south side of the Altai Mountains the eastern Junggar Block of the Kazakhstan-Junggar Plate is linked to the Siberian Plate by the Erqisi Suture Zone (ESZ, Figure 1a [e.g., *Xiao et al.*, 1992]). In general, the collage of terranes comprising the Altai Mountains appears to have been formed by strike-slip deformation resulting from Late Devonian–Early Carboniferous collision of the Altai-Mongolian terrane and the Siberian Plate, and from Late Carboniferous–Permian collision of the Kazakhstan-Junggar and Siberian Plates [e.g., *Xiao et al.*, 1992; *Buslova et al.*, 2004].

[7] The Halaqiaola basalts are located just north of the ESZ, about 50 km east of Fuyun city (Figure 1b). In general, the lava flows are horizontal and the succession overlies Proterozoic basement with a thickness exceeding 50 m. The lavas are mostly fresh and can be divided into at least three rhythms from bottom to top with each rhythm in olivine basalt terminating in a distinctive almond-shaped vesicular basalt unit [*XRSCT*, 1981; *Bureau of Geology and Mineral Resources of Xinjiang Uygur Autonomous Region* (BGMRX), 1993; *Zhang et al.*, 1994]. The Halaqiaola basalts were originally thought to be one branch of an extensive zone of Jurassic magmatic activity in the northern Xinjiang region of the Altai Mountains [*TRGSX*, 1978a; *XRSCT*, 1981]. However, according to reinvestigation of the flows [*BGMRX*, 1993] and a whole rock Ar-Ar age of 17.59 ± 0.05 Ma [*Zhang et al.*, 1994], they have subsequently been reinterpreted as a product of Miocene magmatic activity, which is likely to be either part of magmatism linked to the Cenozoic Baikal-Mongolian rift, or to a western extension of the Altai–Inner Mongolian–Xingkai Cenozoic continental magmatic province [*BGMRX*, 1993; *Zhang et al.*, 1994].

[8] According to our field investigation of the Halaqiaola basalts at least five discrete flows are distinguishable and these were selected for both paleomagnetic and geochronological sampling (Figure 1c). Altogether 17 sites were sampled in the basalts with two sites generally collected from each discrete flow discernible in the field. Flow units with a large thickness likely to be composed of two or more flow units were sampled at additional sites (Figure 1c and Table 1). Three basalt block samples were also collected for $^{40}Ar/^{39}Ar$ dating from the vicinities of paleomagnetic sampling sites k02, k08, and k17 and denoted k02Ar, k08Ar, and k17Ar, respectively. All paleomagnetic samples were collected with a portable gasoline-powered drill and oriented by sun compass. Bedding attitudes are generally near horizontal and determined using a magnetic compass with correction for a local declination anomaly of 3° at the sampling site.

[9] In addition, five red bed sites (f18–f21) were collected from a road cut just south of Fuyun city (Figure 1b and Table 1). This sampling area probably belongs to the ESZ at the southern margin of the Altai Mountains (Figure 1a) but some researchers consider that it is structurally integral with the northern margin of the Junggar Block [e.g., *BGMRX*, 1993; *Ye et al.*, 2001a]. The sampled rocks are red to dark red argillaceous sandstones and are assigned to

Table 1. Site-Mean Paleomagnetic Results From the Tertiary Basalt Flows and Red Beds of the Altai Mountains, Northern Xinjiang[a]

Site ID	Strike/Dip	*n*/*N*	D_g	I_g	D_s	I_s	*k*	α_{95}
Haraqiaola Miocene Basalt Flows (N46.91°, E90.02°)								
k01	240/7	8/10	202.7	−70.6	190.0	−65.8	152.4	4.5
k02	240/7	9/9	191.6	−75.4	178.7	−69.7	330.9	2.8
k03	240/7	9/10	186.2	−77.3	173.8	−71.1	295.3	3.0
k04	240/7	8/11	197.8	−72.6	185.1	−67.3	139.8	4.7
k05	240/7	7/10	196.2	−73.2	183.5	−67.8	267.0	3.7
k06	240/7	8/10	201.9	−82.7	176.8	−77.1	145.9	4.6
k07	240/7	6/8	213.0	−45.3	207.3	−41.7	41.7	10.5
k08	240/7	4/8	228.0	−44.8	221.5	−43.0	45.3	13.8
k09	240/7	5/8	262.9	−41.3	256.9	−43.7	139.5	6.5
k10	240/7	6/8	242.8	−35.4	237.8	−35.4	170.0	5.2
k11	240/7	5/9	195.0	−66.9	185.6	−61.5	139.5	6.5
k12	240/7	7/9	208.4	−69.7	195.1	−65.3	356.6	3.2
k13	240/7	8/9	209.5	−68.0	196.9	−63.8	213.3	3.8
k14	133/23	5/8	177.0	−53.0	142.4	−64.0	83.9	8.4
k15	133/23	8/8	196.0	−47.2	174.2	−65.8	169.8	4.3
k16	240/7	8/9	195.0	−72.8	182.9	−67.3	163.8	4.3
k17	240/7	9/11	253.2	−74.1	228.4	−74.2	91.8	5.4
Averaging by sites		17/17	213.7	−65.3			19.0	8.4
					201.0	−64.6	19.6	8.3
Fuyun Paleocene to Eocene Red Beds (N46.96°, E89.53°)								
f18	343/7	9/9	225.1	−40.0	227.5	−34.7	64.8	6.4
f19	343/7	7/8	210.7	−35.8	213.7	−30.5	175.2	4.6
f20	343/7	7/8	198.1	−40.6	202.6	−36.4	41.0	9.5
f21	343/7	9/9	221.7	−46.4	225.0	−40.3	61.3	6.6
f22	343/7	6/6	227.6	−38.4	229.6	−32.0	91.7	7.0
Averaging by sites		5/5	216.6	−41.0			64.9	9.6
					219.7	−35.2	65.3	9.5

[a]Site ID, site identification; strike/dip, strike azimuth and dip of bed; *n*/*N*, number of samples used to calculate the site mean/samples demagnetized; D_g, I_g (D_s, I_s), declination and inclination of direction in situ (after tilt adjustment); *k*, precision parameter of Fisher statistics; α_{95}, radius of cone of 95% confidence about the resultant vector.

the Honglishan Formation originally thought to be Paleocene to Eocene in age and overlain by the Eocene to Oligocene Ulunguhe Formation [*TRGSX*, 1978b]. Because some stratigraphers consider that the overlying Ulunguhe Formation was deposited during the late Cretaceous [e.g., *XRSCT*, 1981; *Tong et al.*, 1990], the Honglishan Formation could be Mesozoic in age. Nevertheless, recent biostratigraphic investigations provided crucial constraints from mammalian fossils supporting an Eocene to Oligocene age assignment for the Ulunguhe Formation in the Ulungur River area of the northern Junggar [*Ye et al.*, 2001a, 2001b] and therefore indicating that the age of the Honglishan Formation is most likely to be Paleocene to Eocene [*BGMRX*, 1993]. Again samples were collected with a portable gasoline-powered drill and oriented by sun compass. Bedding tilts are low and typically northwestward with dips less than 10° (Table 1).

3. Geochronological Analytical Methods and Results

[10] Three fresh whole rock samples k02Ar, k08Ar, and k17Ar were crushed and disintegrated. After sieving, rock chips in the size range of 80–100 mesh (200–120 μm) were ultrasonically cleaned in distilled water, dried, and then handpicked to remove visible contamination. Fresh matrix was wrapped in aluminum foil and irradiated together with Ga1550-biotite standards, optical CaF_2 and K-glass monitors in position H8 of the 49-2 reactor, Beijing, China, for 28.5 hours with a 0.5 mm cadmium foil shield. The reference age for Ga-1550-biotite is 98.79 ± 0.96 Ma [*Renne et al.*, 1998]. Ca, K correction factors were calculated from the CaF_2 and K-glass monitors: $[^{40}Ar/^{39}Ar]_K = 62 \times 10^{-4}$, $[^{39}Ar/^{37}Ar]_{Ca} = 7.92 \times 10^{-4}$, $[^{36}Ar/^{37}Ar]_{Ca} = 2.21 \times 10^{-4}$.

[11] Total fusion of standards and step-heating analyses of samples were performed at the Paleomagnetism and Geochronology Laboratory in the Institute of Geology and Geophysics, Chinese Academy of Sciences (PGL-IGGCAS), Beijing, on a MM5400 mass spectrometer operating in a static mode. The data were corrected for system blanks, mass discriminations, interfering Ca, K derived argon isotopes, and the decay of ^{37}Ar since the time of the irradiation. The decay constant used throughout the calculations is $\lambda = [5.543 \pm 0.010] \times 10^{-10}$ yr^{-1} [*Steiger and Jäger*, 1977]. Details of the analysis and data processing procedures are outlined by *He et al.* [2004]. The results of $^{40}Ar/^{39}Ar$ experiments are summarized in Table 2 and plotted as age spectrum and isotope correlation diagrams in Figure 2.

[12] The matrix from sample k02Ar yields a concordant age spectrum (Figures 2a and 2b). Thirteen successive steps, which account for 97.8% of the total ^{39}Ar released, define a plateau age of 17.06 ± 0.12 Ma (2σ). An inverse isochronal age of 17.27 ± 0.29 Ma (2σ, mean square weighted deviation (MSWD) = 9.2), calculated from all steps comprising the plateau is in good agreement with the plateau age. The $^{40}Ar/^{36}Ar$ intercept of 290.2 ± 4.7 (2σ) is not distinguishable from the air ratio, indicating that no apparent excess argon contamination is present (Figure 2b). Hence 17.27 ± 0.29 Ma (2σ) is the preferred estimate of the eruption age of sample k02Ar.

Table 2. The $^{40}Ar/^{39}Ar$ Analytical Data for Samples From the Halaqiaola Basalt Flows, the Altai Mountains, Northern Xinjiang

Temp, °C	$^{39}Ar/^{40}Ar$ ±2 SD, $\times 10^{-2}$	$^{36}Ar/^{40}Ar$ ±2 SD, $\times 10^{-3}$	Ca/K	^{39}Ar Cum, %	$^{40}Ar^*$, %	$^{40}Ar^*/^{39}Ar$	Apparent Age ±2 SD, Ma
k02Ar Matrix, Weight = 27.53 mg, J = 0.00622 ± 0.00005							
650	10.49 ± 0.03	3.01 ± 0.02	0.8	0.6	11.1	1.06	11.85 ± 1.44
730	17.26 ± 0.02	2.67 ± 0.02	0.6	2.2	21.2	1.23	13.70 ± 0.79
800	28.00 ± 0.03	1.94 ± 0.01	0.3	6.0	42.6	1.52	16.98 ± 0.40
850	37.59 ± 0.05	1.42 ± 0.01	0.1	15.9	57.9	1.54	17.21 ± 0.33
900	37.96 ± 0.02	1.41 ± 0.01	0.1	25.1	58.2	1.53	17.12 ± 0.31
950	46.22 ± 0.02	0.98 ± 0.01	0.2	36.6	71.0	1.54	17.15 ± 0.29
1000	46.35 ± 0.03	0.98 ± 0.01	0.2	47.5	70.9	1.53	17.10 ± 0.29
1050	40.30 ± 0.03	1.30 ± 0.01	0.3	55.7	61.6	1.53	17.07 ± 0.31
1100	20.48 ± 0.01	2.34 ± 0.01	1.1	68.0	30.8	1.50	16.77 ± 0.54
1150	21.00 ± 0.01	2.33 ± 0.01	1.2	79.7	31.2	1.48	16.59 ± 0.54
1200	5.34 ± 0.00	3.13 ± 0.02	4.7	88.9	7.5	1.41	15.72 ± 2.36
1250	4.94 ± 0.01	3.15 ± 0.02	4.8	97.1	6.9	1.39	15.51 ± 2.70
1300	4.06 ± 0.01	3.17 ± 0.02	7.2	98.5	6.2	1.53	17.07 ± 3.26
1350	0.31 ± 0.00	3.37 ± 0.02	6.0	99.5	0.3	0.99	11.09 ± 43.15
1500	0.17 ± 0.00	3.38 ± 0.02	6.0	100.0	0.1	0.56	6.23 ± 80.84
k08Ar Matrix, Weight = 27.56 mg, J = 0.00616 ± 0.00005							
650	20.22 ± 0.06	2.69 ± 0.03	0.8	0.7	20.5	1.01	11.24 ± 0.88
730	29.08 ± 0.05	1.97 ± 0.02	0.5	2.4	41.9	1.44	15.93 ± 0.44
800	36.06 ± 0.02	1.50 ± 0.01	0.3	7.6	55.7	1.54	17.07 ± 0.34
850	45.79 ± 0.03	1.00 ± 0.01	0.2	15.5	70.5	1.54	17.03 ± 0.30
900	48.99 ± 0.34	0.80 ± 0.01	0.1	24.1	76.5	1.56	17.26 ± 0.43
950	49.96 ± 0.05	0.77 ± 0.01	0.2	36.5	77.3	1.55	17.11 ± 0.29
1000	49.04 ± 0.07	0.81 ± 0.01	0.2	46.7	75.9	1.55	17.13 ± 0.30
1050	52.94 ± 0.26	0.70 ± 0.01	0.6	58.7	79.4	1.50	16.60 ± 0.32
1100	45.89 ± 0.03	1.04 ± 0.01	0.7	69.1	69.3	1.51	16.72 ± 0.29
1150	47.45 ± 0.04	1.06 ± 0.01	4.5	80.9	68.8	1.45	16.04 ± 0.29
1200	39.63 ± 0.03	1.45 ± 0.01	4.7	91.3	57.2	1.44	15.97 ± 0.31
1250	4.14 ± 0.01	3.19 ± 0.02	8.6	93.4	5.8	1.40	15.48 ± 3.19
1300	3.88 ± 0.03	3.14 ± 0.02	13.4	93.8	7.2	1.86	20.53 ± 3.39
1350	6.16 ± 0.06	3.01 ± 0.02	13.2	99.3	11.2	1.82	20.08 ± 2.08
1500	3.25 ± 0.01	3.19 ± 0.02	10.9	100.0	5.8	1.78	19.72 ± 4.20
k17Ar Matrix, Weight = 26.28 mg, J = 0.00619 ± 0.00005							
650	18.48 ± 0.14	2.73 ± 0.02	0.9	1.2	19.4	1.05	11.71 ± 0.72
700	23.81 ± 0.12	2.31 ± 0.02	0.7	2.6	31.9	1.34	14.88 ± 0.69
770	37.48 ± 0.07	1.36 ± 0.01	0.4	6.6	59.8	1.59	17.72 ± 0.37
830	43.05 ± 0.04	1.10 ± 0.01	0.2	16.2	67.5	1.57	17.42 ± 0.31
880	54.78 ± 0.03	0.53 ± 0.00	0.1	31.3	84.2	1.54	17.09 ± 0.28
930	55.75 ± 0.07	0.46 ± 0.01	0.2	41.9	86.5	1.55	17.23 ± 0.29
980	57.86 ± 0.19	0.37 ± 0.01	0.2	51.5	89.1	1.54	17.12 ± 0.31
1030	54.90 ± 0.06	0.53 ± 0.01	0.3	62.0	84.2	1.53	17.05 ± 0.29
1080	59.58 ± 0.05	0.34 ± 0.01	0.4	71.1	90.0	1.51	16.80 ± 0.28
1130	60.81 ± 0.06	0.32 ± 0.00	0.7	81.1	90.6	1.49	16.57 ± 0.27
1180	59.67 ± 0.04	0.52 ± 0.01	5.6	92.0	84.6	1.42	15.76 ± 0.27
1250	53.45 ± 0.08	1.00 ± 0.01	16.4	99.4	70.4	1.32	14.66 ± 0.29
1350	31.73 ± 0.38	1.96 ± 0.03	29.9	99.9	42.0	1.32	14.72 ± 0.86
1500	10.76 ± 0.83	2.83 ± 0.06	33.7	100.0	16.5	1.53	17.05 ± 4.35

[13] The matrix from sample k08Ar yields a slightly disturbed age spectrum (Figures 2c and 2d), whereas matrix from sample k17Ar gives a slightly decreasing age spectrum at higher temperatures with a maximum age of 17.7 Ma in the lower temperature steps and a minimum age of 14.7 Ma in the higher temperature steps (Figures 2e and 2f). Notwithstanding this, the five successive steps, which account for 44.3% and 55.5% of the total ^{39}Ar released, define plateau ages of 17.11 ± 0.14 Ma (2σ) and 17.18 ± 0.13 Ma (2σ). The inverse isochronal ages of 17.16 ± 0.17 Ma (2σ, MSWD = 0.95) and 17.06 ± 0.41 Ma (2σ, MSWD = 4.5), calculated from the five steps forming the plateaus accord with the plateau ages. The $^{40}Ar/^{36}Ar$ intercepts of 292.7 ± 6.8 (2σ) and 305 ± 38 (2σ) are close to the air ratio and indicative of no apparent excess argon contamination (Figures 2d and 2f). Hence 17.16 ± 0.17 Ma (2σ) and 17.06 ± 0.41 Ma (2σ) are the preferred eruption ages of samples k08Ar and k17Ar.

[14] The consistent $^{40}Ar/^{39}Ar$ ages of k02Ar (17.27 ± 0.29 Ma), k08Ar (17.16 ± 0.17 Ma), and k17Ar (17.06 ± 0.41 Ma) indicate that there is no apparent excess argon contamination and little alteration and therefore that 17 Ma can be reliably accepted as the eruption age of the Halaqiaola basalts.

4. Paleomagnetic Analysis

[15] Following sample trimming, a single cylinder from each field core was first used to measure the anisotropy of magnetic susceptibility employing a KLY 3 kappa bridge.

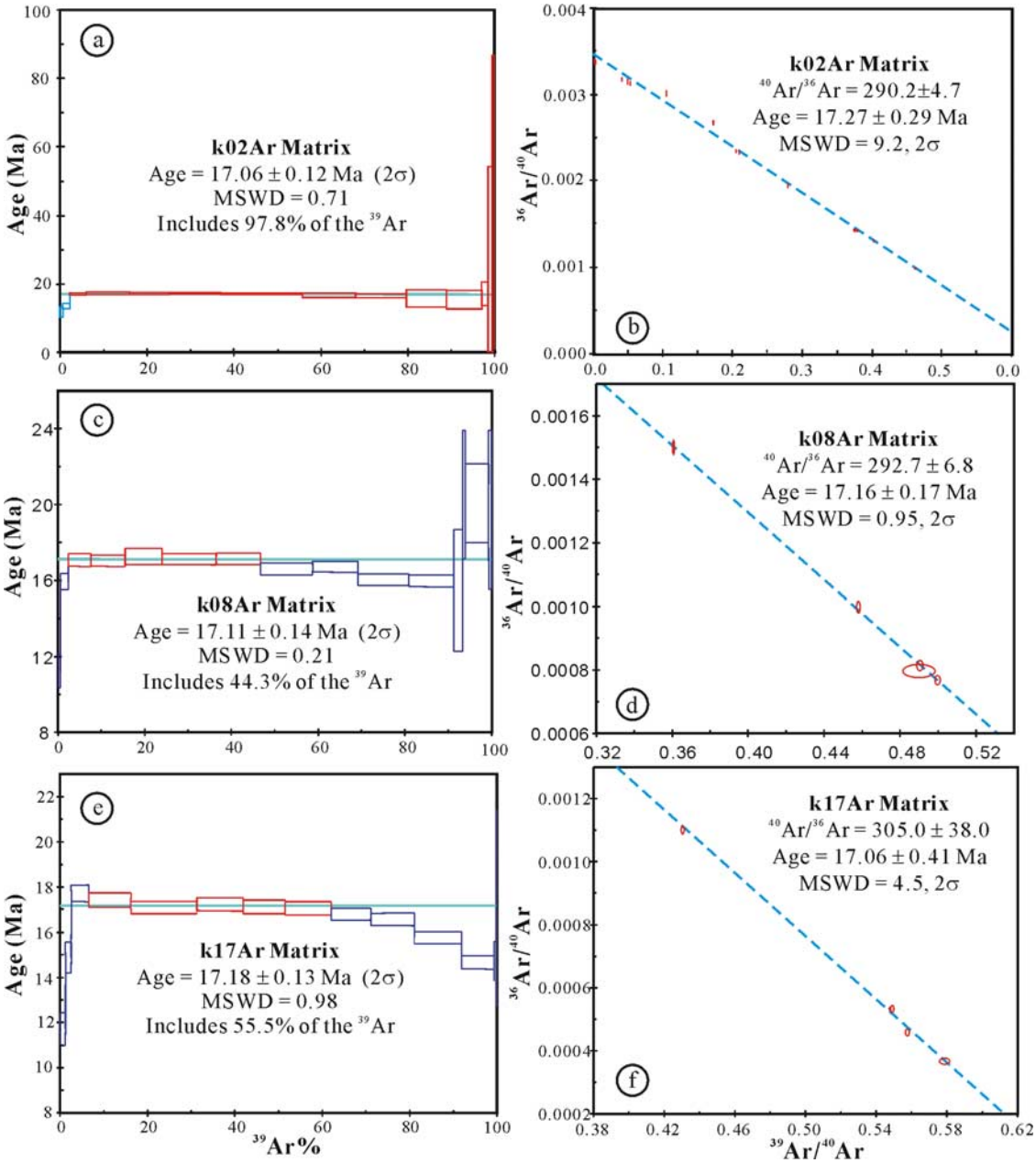

Figure 2. Apparent age spectrum and isochron diagrams derived from $^{40}Ar/^{39}Ar$ analysis of samples (a, b) k02Ar, (c, d) k08Ar, and (e, f) k17Ar. All errors are shown at the 2σ level.

All specimens were then subjected to either progressive thermal or alternating field (AF) demagnetization. Progressive thermal demagnetization was carried out in a TD-48 thermal demagnetizer with residual magnetic field of less than 10 nT in the cooling chamber. For the red bed samples, thermal demagnetization was performed in steps of 50°C to 550°C, and subsequently in steps of 20°C or 10°C to Curie points of the remanence carriers. For the basalt samples, thermal intervals were reduced to 15°C or 20°C at demagnetization temperatures above 250°C. The AF demagnetization was conducted using a 2G600 AF demagnetizer coupled to a 2G-760 U-channel system in steps of 2.5 to 15 mT to peak fields up to a maximum of 100 mT. Remanences were measured by JR-5A spinner magnetometer, 2G-755R cryogenic magnetometer, and 2G-760 U-channel system in the PGL-IGGCAS where magnetometers and demagnetizers are installed in a field-free space (<300 nT). Demagnetization results were converted into orthogonal diagrams [*Zijderveld*, 1967] and stereographic projections to resolve component structures by principal component analysis [*Kirschvink*, 1980]; means were calculated for each site using standard Fisher statistics [*Fisher*, 1953]. Some basalt core end material was subjected to thermomagnetic analysis of remanence (remanence versus temperature curves) using a variable field translation balance (VFTB). Low-temperature properties and hysteresis

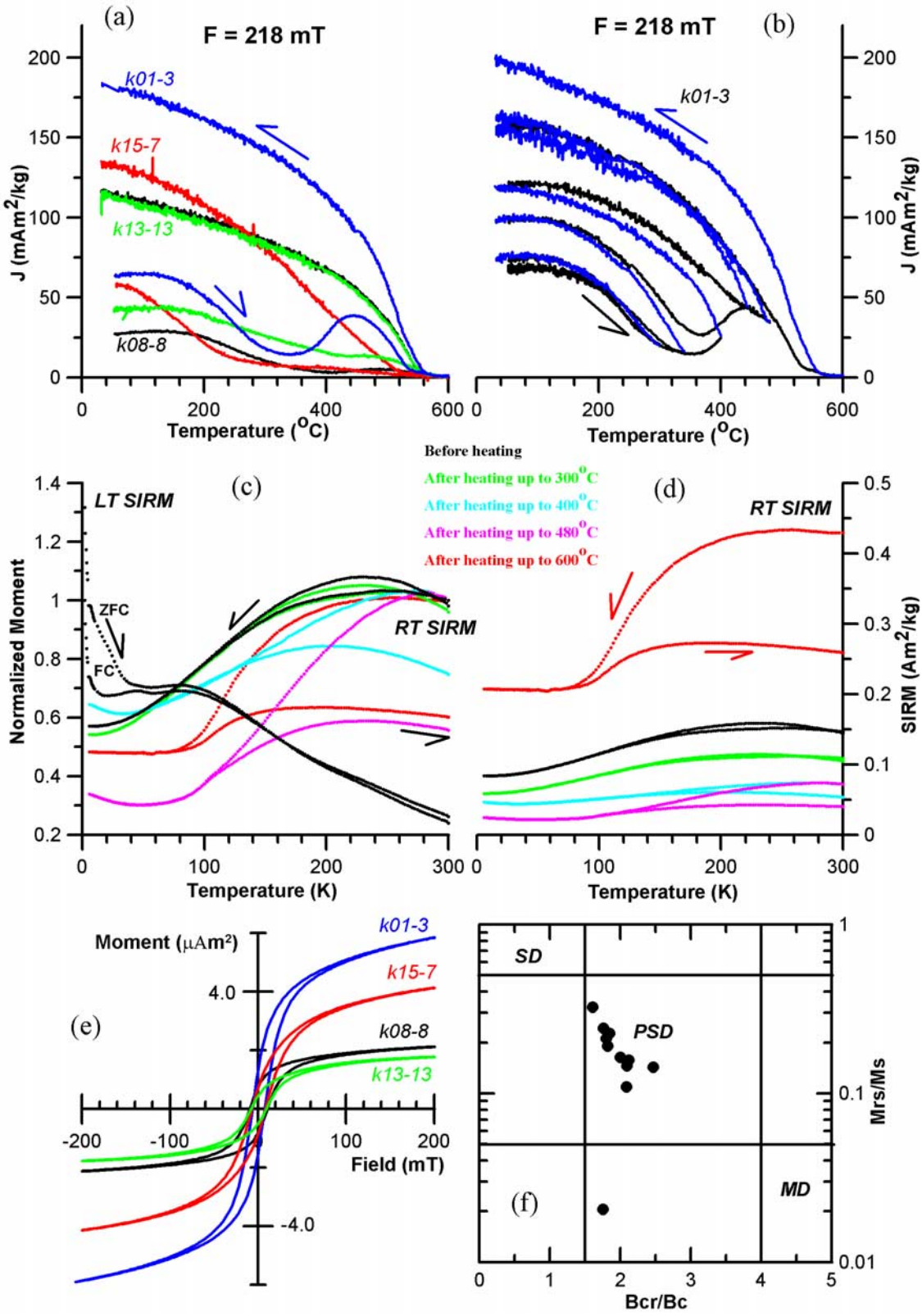
(a)
F = 218 mT
k01-3
k15-7
k13-13
k08-8
J (mAm2/kg)
Temperature (°C)
(b)
F = 218 mT
k01-3
J (mAm2/kg)
Temperature (°C)
Before heating
After heating up to 300°C
After heating up to 400°C
After heating up to 480°C
After heating up to 600°C
(c)
LT SIRM
ZFC
FC
RT SIRM
Normalized Moment
Temperature (K)
(d)
RT SIRM
SIRM (Am2/kg)
Temperature (K)
(e)
Moment (μAm2)
k01-3
k15-7
k08-8
k13-13
Field (mT)
(f)
SD
PSD
MD
Mrs/Ms
Bcr/Bc

Figure 3

parameters for some pilot basalts were also measured using a Quantum Designs model MPMS XP-5 magnetic properties measurement system and a Princeton/MicroMag model 2900 alternating gradient magnetometer, respectively, in the PGL-IGGCAS.

5. Paleomagnetic Results

5.1. The Halaqiaola Basalts

[16] Thermomagnetic curves (*J-T*) of powdered samples from each site show a common feature with the cooling curve far above the heating curve up to a temperature of 600°C (Figure 3a), indicative of a formation of new ferromagnets with high magnetization during the heating. The main drop of magnetization occurred at ~300°–400°C in the majority of samples (e.g., samples k01-3, k08-8, and k15-7 in Figure 3a) and at ~400°–530°C in a minority of samples (e.g., sample k13-13 in Figure 3a). Further progressive J-T curves at a series of increasing peak temperatures show that the J-T curve is reversible when the peak temperature is lower than the distinct Curie temperature, determined as the intersection of the first descending segment in the heating curve with the tangent of the subsequent paramagnetic tail (Figure 3b). These magnetic properties indicate that magnetochemical changes occur at heating to temperatures higher than the Curie temperature and suggest that titanomagnetite or titanomaghemite is the predominant ferromagnet in the basalts. This view and the exsolution of titanomagnetite or titanomaghemite to magnetite when heating above the Curie temperature are confirmed by low-temperature cooling and warming behaviors of saturation isothermal remanence (SIRM). The reversible behavior of the room temperature SIRM for the unheated sample and the sample just heated up to 300°C, with a maximum SIRM around 220–240 K (Figure 3c), probably reflects the temperature dependence of SIRM in titanomagnetite and titanomaghemite [*Schult*, 1968; *Krasa*, 2002]. The clear appearance of the Verwey transition in the SIRM at ~120 K, as well as the greatly enhanced SIRM intensity in the sample heated up to 600°C (Figure 3d), describe the trajectory of exsolution of ferromagnets to magnetite with increasing peak heating temperatures [e.g., *Ozdemir et al.*, 2002]. On the other hand, a difference below 50 K between two warming curves of low-temperature SIRM produced following a zero-field cooling (ZFC) and a 5.0 T magnetic field cooling (FC) (Figure 3c) indicates that some high-Ti hemoilmenites are included in the basalts (M. Jackson, personal communication, 2004). However, the presence of hemoilmenite can be ignored in the paleomagnetic analysis because it will not contribute to the remanence above room temperature [*Krasa*, 2002]. In addition, a Day diagram [*Day et al.*, 1977] of room temperature hysteresis parameters for pilot samples indicates that the carriers of remanence are within the pseudosingle-domain range with a coercivity of about 10 mT (Figures 3e and 3f), although we note that the values of domain states estimated from room temperature hysteresis parameter ratios have been questioned [e.g., *Goguitchaichvili et al.*, 2001].

[17] Initial natural remanent magnetizations (NRMs) of the basalt specimens give a clear separation of the 17 sites into two groups. The first group comprises sites k01–k06 and k11–k17 with NRMs ranging from 0.107 to 2.060 A m^{-1} and an average value of 0.640 A m^{-1}. Another group comprising the remaining four sites (k07–k10) has a much higher average value (99.561 A m^{-1}) of initial NRM with values ranging from 7.120 A m^{-1} to 2.182×10^2 A m^{-1}. We interpret these differences in terms of variations in magnetic composition and/or proportion of ferromagnets in the specimens. Comparison of thermal and AF demagnetization of pilot specimens from each site shows that AF demagnetization yields a valid component analysis at all sites (Figures 4a–4f), while the thermal demagnetization is successful at resolving stable magnetizations in specimens from sites k07–k10 (Figures 4h and 4i) and few specimens from k01–k06 and k11–k17 (Figure 4g). Because of the evident success of the AF demagnetization, all remaining specimens from k01–k06 and k11–k17 and about half the specimens from k07–k10 were subjected to this treatment, while the remaining specimens from k07–k10 were subjected to thermal demagnetization. In general, characteristic remanent magnetizations (ChRMs) could be identified following removal of a low-coercivity/unblocking temperature remanence at peak alternating fields below 10–15 mT (Figures 4a–4f) or peak demagnetization temperatures below 180°–220°C (Figures 4g–4i). The ChRM directions for specimens from k01–k06 and k11–k17 were defined by AF demagnetization between 20 mT and 80–100 mT (Figures 4a–4d), while a few specimens from sites k13, k15, and k16 yielded ChRM directions unblocked between 220 and 300°–385°C (Figure 4g). Specimens from sites k07–k10 yield ChRM directions isolated by alternating fields of 20 mT to 80–100 mT (Figures 4e and 4f), while thermal demagnetization identifies a much higher unblocking temperature of some 550°C for the ChRM component although over 90% of the initial NRM had been removed by temperature steps up to 275°–300°C (Figures 4h and 4i). This demagnetization behavior may indicate that the ChRM resides both in high-Ti titanomagnetite and poor-Ti titanomagnetite. All ChRM directions except one recorded in a specimen from k08 are of reversal polarity. Excluding some specimens showing large deviation from the remaining site populations, mean directions of each site are accurately

Figure 3. (a) Representative results of thermomagnetic analysis of remanence (J-T curves) of samples from several Halaqiaola basalt flows. (b) Progressive J-T curves for basalt sample k01–3 showing progressive elimination of the low Curie point with repeated heating-cooling cycles. All the J-T curves were measured in an argon gas atmosphere with heating and cooling rates of ~10°C min^{-1}; a steady magnetic field of 218 mT was applied for acquisition of remanence. (c, d) Low-temperature properties of basalt sample k01-3. Room temperature (RT) and low-temperature (LT) saturation isothermal remanence (SIRM) were produced by a higher DC magnetic field of 5.0 T in 300 and 2 K, respectively. (e) Representative hysteresis loop of samples from basalt flows with maximum field of 1.0 or 1.5 T. The illustrated plots show the segment of the loops below 200 mT. (f) Day plot [*Day et al.*, 1977] of hysteresis parameters for samples from the basalt flows.

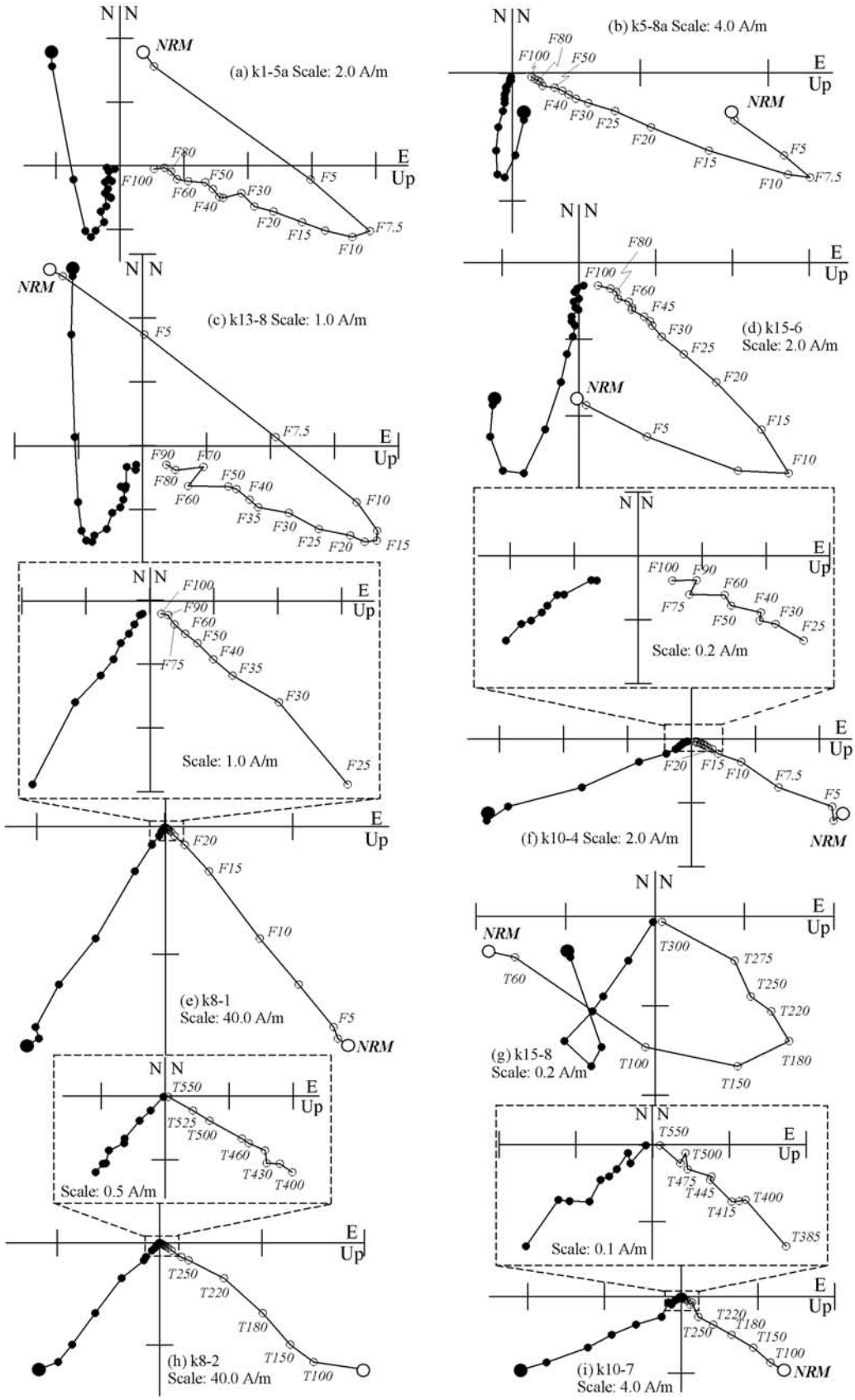

Figure 4. Representative orthogonal vector plots for the basalt specimens. Directions are plotted in situ; solid and open circles represent vector endpoints projected onto the horizontal and vertical planes, respectively. T and F indicate thermal (°C) and AF (mT) demagnetizations, respectively.

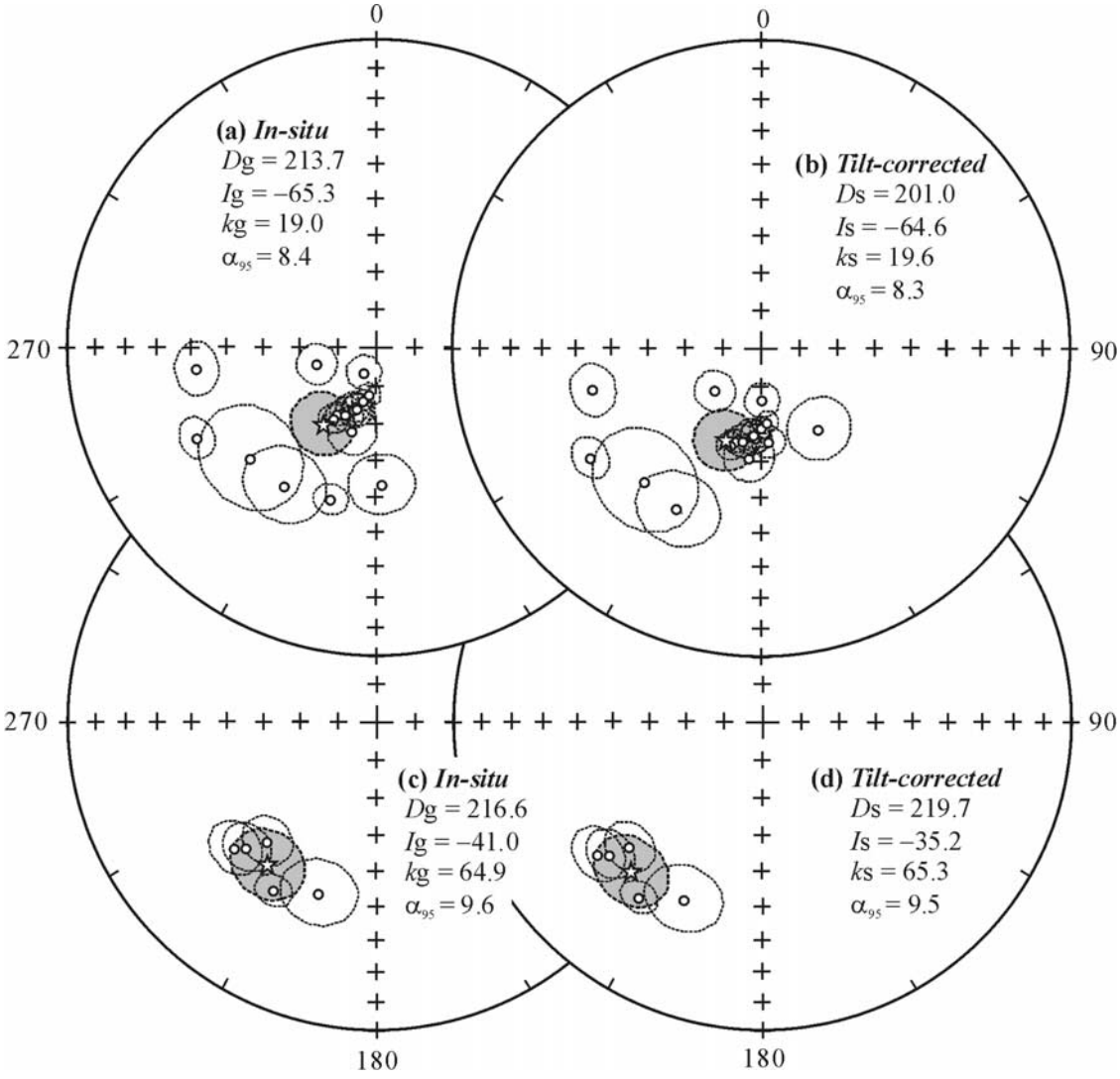

Figure 5. Equal-area projections of site-mean directions of ChRM before and after tilt adjustment for (a, b) Halaqiaola basalts and (c, d) Fuyun red beds. Solid/open symbols represent downward/upward inclinations; stars indicate the overall mean directions with the 95% confidence limits.

defined with the exception of two sites (k07 and k08) with 95% confidence cones greater than 10° (Table 1). Fisher statistics [*Fisher*, 1953] applied to the 17 site-mean directions yield a tilt-corrected mean of $D = 201.0°$, $I = -64.6°$, $\alpha_{95} = 8.3°$ (Figure 5b and Table 1).

5.2. Fuyun Red Beds

[18] Forty specimens were subjected to thermal demagnetization up to a maximum temperature of 686°C in 17 steps and 38 specimens yielded stable demagnetization trajectories (Figure 6). The ChRM is generally isolated following removal of viscous and/or secondary remanence by demagnetization below 240°–350°C (Figures 6b–6d), except for a few specimens that show a much higher unblocking temperature of the secondary magnetization (Figure 6a). The high-temperature ChRM was subtracted between 400/450°C and 675/686°C (Figures 6b–6d) in the majority of samples and between 580°C and 675/686°C in a minority (Figure 6a), indicating that hematite is the magnetic carrier of the ChRM. These ChRM components have uniform reversed polarity (Figures 5c and 5d). Site-mean observations are well determined with the 95% confidence limits less than 10°, and they provide a group mean of $D = 219.7°$, $I = -35.2°$ with $k = 65.3$ and $\alpha_{95} = 9.5°$ (Figure 5d and Table 1). A fold test is not possible here because the bedding dips are essentially uniform (Table 1). Whether this remanence is a postdeposition detrital remanent magnetization (PDRM) or a later chemical remanent magnetization (CRM) depends on the paragenesis of the hematite carrier. We have examined magnetic fabrics (section 5.3) to help evaluate this question.

5.3. Anisotropy of Magnetic Susceptibility

[19] The anisotropy of magnetic susceptibility (AMS) determined from 123 basalt specimens and 36 red bed specimens displays contrasting character in the two rock facies (Figure 7). The basalt specimens have very low corrected anisotropy degrees (P_j) with a majority of less than 1.02 and no tendency for oblate or prolate shapes to prevail (Figure 7a). The principle anisotropy directions are

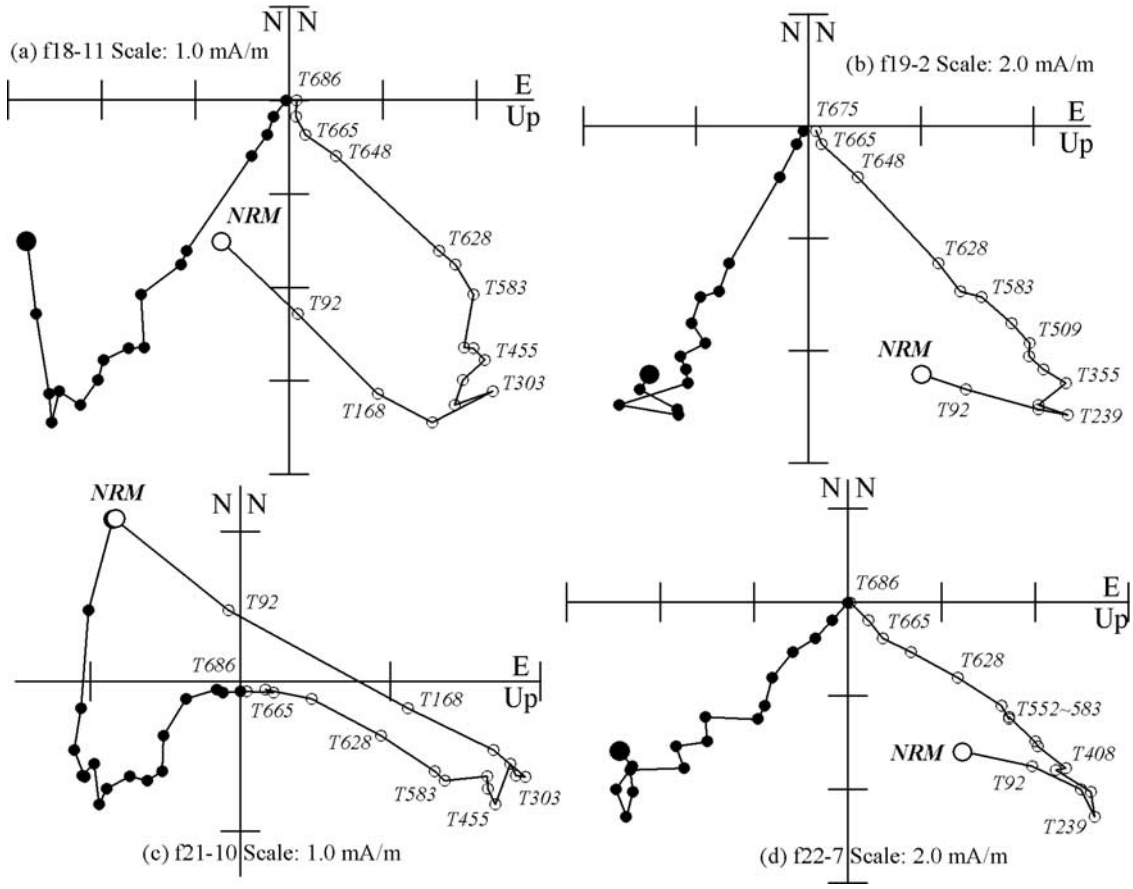

Figure 6. Typical orthogonal vector plots illustrating thermal demagnetization behavior of Fuyun red beds. Symbols are as for Figure 4.

dispersed with a weak tendency for the k_{max} axes to lie in a NE-SW girdle and some k_{min} axes to lie in a subhorizontal NW-SE azimuth at right angles (Figure 7c). The red bed specimens show relatively large anisotropy degrees (P_j) with a majority in the range 1.04 to 1.06 and an average value of 1.054 (Figure 7a). The red bed specimens also show oblate shapes with an average value of shape parameter (T) of 0.806 (Figure 7a). The minimum principle anisotropy directions are oriented perpendicular to the bedding, while the maximum principle directions are nearly horizontal and trend roughly N–S (Figure 7b). The very low degrees of anisotropy and large scatter of AMS principle directions in the basalt specimens, which is also observed in the Cretaceous and Paleogene basalts in the Tuoyun Basin of the southwest Tian Shan Range [*Gilder et al.*, 2003; *Huang et al.*, 2005], suggest that the Halaqiaola basalts have experienced no significant straining due to tectonic stress and probably preserve a primary flow fabric (Figure 7c). The magnetic fabric of the red bed samples is predominant a depositional fabric [e.g., *Hrouda*, 1982] as indicated by very low q factors (having an average of 0.104) and f factors (angles between the minimum principle directions and bedding pole are mostly lower than 10°) (Figure 7b). Noting that the red bed specimens also show relatively low anisotropy degrees (Figure 7a) suggests that they are unlikely to have experienced significant straining, and compaction is also unlikely to be a major influence on fabric [e.g., *Hrouda*, 1982]. The dominant N-S alignment of k_{max} axes within the bedding close to the predominant direction of Tertiary fluvial systems and perpendicular to the tectonic grain (Figure 7b) suggests that primary deposition is the most important influence on fabric and supports the interpretation of the ChRM as a PDRM.

6. Discussion

[20] The geochronological studies on three samples yield $^{40}Ar/^{39}Ar$ isochron ages of 17.06 ± 0.41, 17.16 ± 0.17, and 17.27 ± 0.29 Ma for three successive horizons in the Halaqiaola basalt succession from northern Xinjiang (section 3) compare well with a published $^{40}Ar/^{39}Ar$ age of 17.59 ± 0.05 Ma [*Zhang et al.*, 1994] and collectively support an extrusion age of ~17 Ma for this magmatic activity. The original assignment of this volcanism to the extensive Jurassic magmatic activity in the Altai Mountains of northern Xinjiang [*TRGSX*, 1978a; *XRSCT*, 1981] can be confidently rejected. Instead, the Halaqiaola basalts together with flows sporadically distributed elsewhere around Halaqiaola village [*TRGSX*, 1978a] are interpreted to be products of an early Miocene magmatic event.

[21] Rock magnetic behaviors and demagnetization properties indicate that titanomagnetite with varying content of titanium is the dominant magnetic carrier of ChRM in the basalts. The AMS results (Figures 7a and 7c) indicate a primary flow fabric for the Halaqiaola basalts without significant straining due to tectonic stress and suggest that

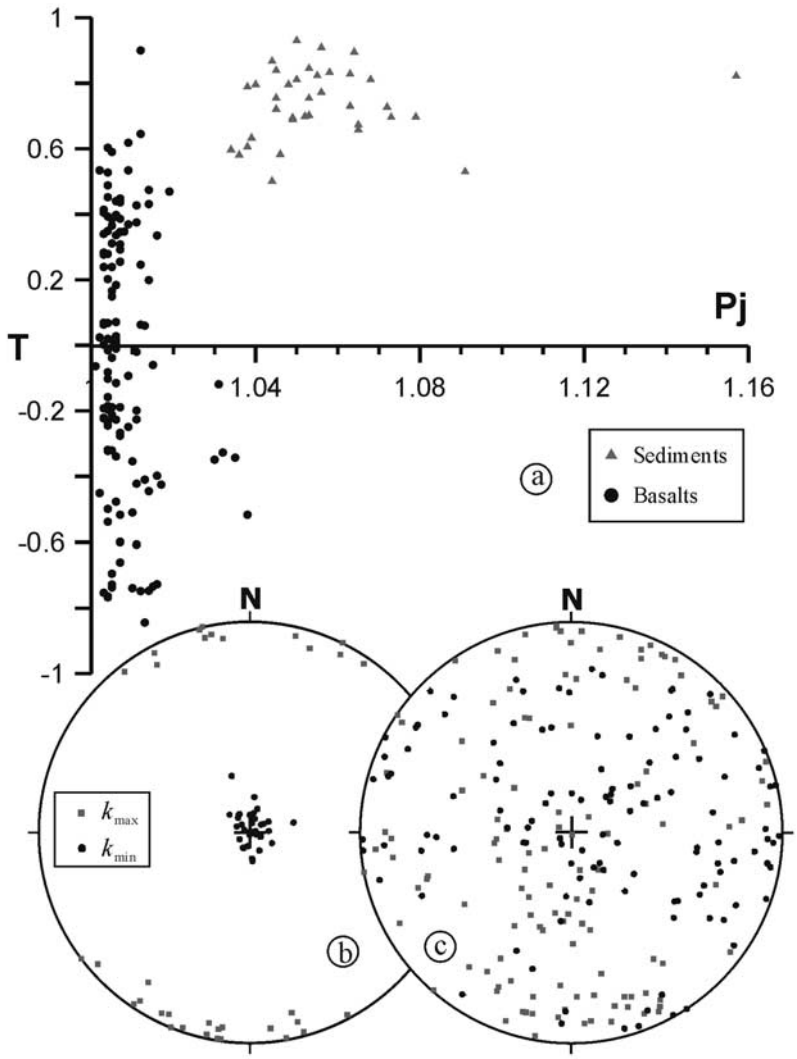

Figure 7. Summary of AMS results. (a) Corrected magnetic susceptibility anisotropy (P_j) versus the magnetic susceptibility ellipsoid shape parameter (T). (b, c) Stereographic projections showing tilt-corrected AMS orientations in Paleocene to Eocene Fuyun red beds (Figure 7b) and Miocene Halaqiaola basalt flows (Figure 7c). Squares and circles show orientations of maximum and minimum principal axes of magnetic susceptibility, respectively. All symbols are plotted on the lower hemisphere.

the accurately defined concordant ChRM directions with uniform reversed polarity probably record a primary magnetization acquired during, or soon after, the lavas cooled through blocking temperatures of the ferromagnets. Although their error limits overlap, the three new radiometric ages are consistent with the flow sequence observed in the field. They permit a correlation with the Geomagnetic Polarity Timescale (GPTS [*Cande and Kent*, 1995]) and indicate that this pulse of magmatic activity occurred mainly during reversed chron C5Cn.3r assigned to the interval 16.7 to 17.3 Ma. The Fisherian overall mean direction derived from 17 sites corresponds to a paleomagnetic pole at 167.6°E, 78.0°N with A_{95} = 7.9° and S = 23.7°. Noting that the virtual geomagnetic pole (VGP) dispersion (S) at a latitude of 47° is predicted to be about 17° for 0 to 5 Ma [*Merrill and McElhinny*, 1983] and that the VGP dispersion in all latitude bands for the interval 5 to 45 Ma is slightly greater than for 0 to 5 Ma [*Butler*, 1992], the dispersion of site-mean VGPs of this study suggests that the group-mean paleopole has adequately sampled geomagnetic secular variation and hence represents a time-averaged paleomagnetic pole.

[22] The well-defined high-temperature characteristic remanence from five sites in Paleocene to Eocene red beds from the vicinity of Fuyun city (Figure 1) yields a paleomagnetic pole at 47.6°N, 206.3°E with K = 54.4 and A_{95} = 10.5°. This paleomagnetic result indicates a high degree of inclination flattening of 25.0 ± 8.7° in these red beds when the overall mean direction is compared with the predicted direction at the sample locality from the 60 Ma reference pole for stable Eurasia [*Besse and Courtillot*, 2002]. This degree of shallowing is approximately consistent with the ~20° of inclination flattening identified in the interval 40 to 60 Ma from central Asian terrestrial sediments [see *Gilder et al.*, 2003, Figure 7]. It is likely to have been induced mainly by compaction effects [e.g., *Tan et al.*, 2003; *Tauxe*, 2005] as suggested by the typical sedimentary AMS fabric and significant anisotropy degrees (Figures 7a and 7b). Hence

Table 3. Compilation of Paleomagnetic Poles From Central Asian Volcanic Rocks From the Region North of Tibet Between Latitudes 35°N to 55°N and Longitudes 70°E to 110°E[a]

No.	Slat, °N	Slong, °E	Age	Mean Age	Plat, °N	Plong, °E	*dp* or A_{95}	*dm*	*N*(*n*)	Reference
1[b]	50.5	105.0	Quaternary	0.5	86.0	180.0	4.2	5.0	1(23)	*Rozinov and Sholpo* [1971], 3827[c]
2[d]	36.2	81.5	K-Ar 1.05–1.44 Ma	1.25	82.2	193.4	3.2	4.4	13(79)	*Otofuji et al.* [1995], 7633[c]
3	36.2	81.5	K/Ar 1.05–1.44 Ma	1.25	79.9	183.1	1.6	2.4	20(120)	*Meng et al.* [1998]
4[b]	51.0	104.0	late Pliocene	2.5	83.0	133.0	4.7	5.3	1(42)	*Davydov and Kravchinsky* [1971], 3985[c]
5[b]	36.3	79.0	K/Ar 12.7 and 5.8 Ma	9.3	88.0	356.8	6.0	8.3	5(29)	*Li et al.* [1995]
6	36.3	78.8	K/Ar 12.7–5.8 Ma	9.3	86.0	22.8	7.5	10.1	5(14)	*Meng et al.* [1998]
7	53.0	103.0	Miocene to Pliocene	~12.5	64.0	245.0	1.7	2.6	1(75)	*Davydov and Kravchinsky* [1971], 3986[c]
8[b]	52.0	101.0	Miocene to Pliocene	~12.5	76.0	241.0	3.4	4.5	10(91)	*Davydov and Kravchinsky* [1971], 3987[c]
9	36.3	79.0	K/Ar 12.7 Ma	12.7	82.4	342.9	5.2	7.3	4(24)	*Li et al.* [1995]
10	36.0	79.2	K/Ar 12.7 Ma	12.7	82.8	343.2	6.9	9.9	4(12)	*Meng et al.* [1998]
11[b]	46.5	96.5	Miocene	~15.0	77.0	162.0	19.2	23.2	4(36)	*Gorshkov et al.* [1991], 7277[c]
12	46.9	90.0	Ar/Ar 17 Ma	17.0	78.0	167.6	10.9		17(120)	this study
13	51.5	103.0	early Miocene	~20.0	80.0	273.0	4.6	6.0	30(71)	*Davydov and Kravchinsky* [1971], 3988[c]
14	43.5	104.5	Oligocene	~30.0	70.0	204.0	8.3	11.5	(20)	*Gorshkov et al.* [1991], 7278[c]
15[b]	40.7	76.1	Eocene circa 54 Ma	54.0	77.0	187.5	4.4		18(94)	*Bazhenov and Mikolaichuk* [2002]
16	42.6	76.4	K/Ar 50–60 Ma	55.0	75.0	220.9	8.7	13.2	4(53)	*Thomas et al.* [1993], 7273[c]
17	40.2	75.3	Ar/Ar 57.2–61.7 Ma	59.5	49.9	162.9	7.4		20(157)	*Huang et al.* [2005]
18[b]	42.0	75.0	K/Ar 55–65 Ma	60.0	76.0	190.0	3.9	5.6	3(32)	*Rozinov and Sholpo* [1971], 4136[c]
19	40.2	75.4	K/Ar 61.7 Ma	61.7	64.6	177.5	12.8	19.2	4(20)	*Li et al.* [1995]
20[d]	40.2	75.3	K/Ar 61.7 Ma	61.7	48.1	142.0	13.4	17.3	5(28)	*Meng et al.* [1998]
21	55.0	90.3	Ar/Ar 74–81 Ma	75.0	78.3	271.0	8.8	11.3	4(33)	*Bragin et al.* [1999], 8824[c]
22	40.2	75.4	K/Ar 112.7 Ma	112.7	77.1	211.8	11.3	17.0	8(46)	*Li et al.* [1995]
23[d]	40.2	75.3	K/Ar 112.7 Ma	112.7	72.6	214.0	10.4	16.4	10(58)	*Meng et al.* [1998]
24[b]	40.2	75.3	Ar/Ar 113 ± 1.6 Ma	113.0	64.1	172.1	12.0		13(89)	*Gilder et al.* [2003], 8955[c]
25	45.0	100.5	Early Cretaceous	~120.0	84.0	129.0	5.5	6.6	(52)	*Gorshkov et al.* [1991], 7279[c]
26	41.5	72.2	Early Cretaceous	~120.0	78.8	234.2	2.0	2.9	5(22)	*Eroshkin* [1991], 7304[c]
27	41.2	104.0	Early Cretaceous	~120.0	71.1	200.5	2.7		7(38)	*Ren et al.* [2004]
28[b]	50.5	107.5	K/Ar 110–120 Ma	120.0	73.0	158.0	6.2	7.1	3(46)	*Rozinov and Sholpo* [1971], 4198[c]
29[b]	41.5	72.2	Hauterivian	133.0	80.0	247.0	1.8	2.7	6(74)	K. A. Abdullaev et al. (Paleomagnetic directions and paleomagnetic pole positions: Data for the former USSR–Issue 8, in Catalogue, VNIGRI Inst., St. Petersburg, unpublished, 1993), 6709[c]

[a]Slat/Slong (Plat/Plong), latitude/longitude of site (pole); *N*(*n*), number of sites (samples) used to calculate the paleopole; *dp*/*dm*, semiaxis of the confidence ellipse about the pole position in the colatitudinal direction and at right angles to it, respectively; A_{95}, radius of circle of 95% confidence about the paleopole.

[b]Results appear in Table 2 of *Gilder et al.* [2003].

[c]Result number in the IAGA Global Paleomagnetic Database (version 4.6, February 2005, http://www.ngu.no/dragon/Palmag/paleomag.htm).

[d]Results recalculated using all the site means in original data Tables 5 and 7 of *Meng et al.* [1998] and Table 1 of *Otofuji et al.* [1995].

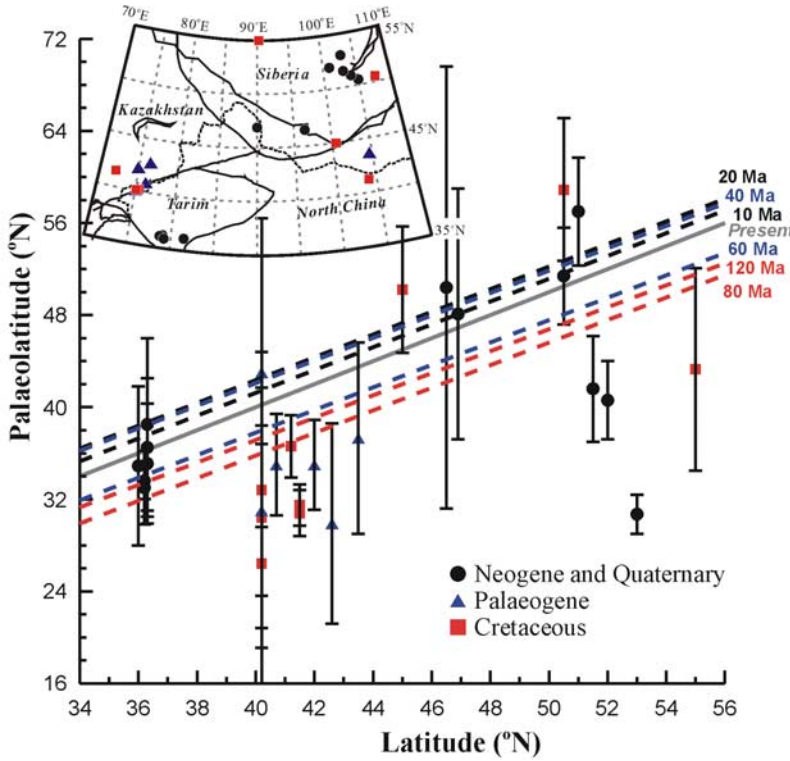

Figure 8. Distributions of paleolatitudes with 95% error limits versus latitudes of sampling site of available paleomagnetic results from Cretaceous and Cenozoic volcanic rocks north of Tibet (latitude 35–55°N, longitude 70–110°E). Paleomagnetic poles obtained from less than 10 samples are excluded from the plot (Table 3). The sloping lines are paleolatitudes predicted at the longitude of central Asia (90°E is used here) at 10 to 40 Myr intervals from Early Cretaceous to the present-day as derived from the master apparent polar wander path of Eurasia [*Besse and Courtillot*, 2002]. Inset is an equal-area projection of sampling locations of paleomagnetic poles in Table 3.

an inclination flattening of ~20° could be more generally present in Paleogene terrestrial sediments from the Altai Mountains and adjoining regions and this emphasizes the need for caution when using paleomagnetic data from this rock facies for tectonic interpretation.

[23] The ~17 Ma paleomagnetic pole obtained from the Halaqiaola basalts shows that they have experienced an insignificant northward latitudinal translation of 1.0 ± 9.0° and little or no counterclockwise (CCW) rotation of 9.4 ± 13.6° with respect to stable Eurasia during the last ~20 Myr [*Besse and Courtillot*, 2002]. The large uncertainty of ~22° ($\sin \Delta D = \sin(\alpha_{95})/\cos(I)$ [*Butler*, 1992]) in the observed mean declination ($D = 21°$) shows that the suggested CCW rotation is paleomagnetically insignificant. The result implies that the Altai Mountains have experienced no significant northward convergence during the last ~20 Myr.

[24] To evaluate possible northward convergence patterns of the central Asian terrenes since onset of the India/Asia collision, we use an updated compilation of Cretaceous and Cenozoic paleomagnetic poles obtained from volcanic rocks north of Tibet (Table 3), with help of the IAGA Global Paleomagnetic Database (version 4.6, February 2005, http://www.ngu.no/dragon/Palmag/paleomag.htm). In this compilation, we accept paleopoles obtained from a location range of latitude 35–55°N and longitude 70–110°E and discard paleopoles obtained from less than 10 specimens. Because of the scarcity of paleomagnetic results from Cretaceous and Cenozoic volcanic rocks within some of the latitude bands in central Asia it is impossible to undertake an analysis of the data in Table 3 using a sliding latitude window technique. Instead we use a paleolatitude versus latitude plot (Figure 8), in which predicted paleolatitudes for the region of central Asia (longitude 90°E is used here) are computed from the Eurasian master curve [*Besse and Courtillot*, 2002]. With the exception of three old paleopoles from the southern margin of the Siberian Plate or northern margin of the Altai Mountains [*Davydov and Kravchinsky*, 1971], which show a 10 to 20° latitude difference with the predicted values, paleolatitudes computed from Neogene and Quaternary paleopoles are consistent with the latitudes predicted from the Eurasian path. The standard deviation of ten Neogene to Quaternary paleolatitudes with the predicted values is within 2.5 ± 7.4° to 2.8 ± 7.5°, relative to present and 20 Ma reference values, respectively. Noting that the Neogene and Quaternary paleopoles are distributed both within the Kunlun and Altai regions of compressive strain (Table 3 and Figure 8) implies that these central Asian terrenes have experienced little or no northward convergence during the last ~20 Myr.

[25] For the Paleogene and Cretaceous time windows, most paleolatitudes plot a further 1–10° south of the latitudes predicted from the Eurasian path during the inter-

val 60–120 Ma, with the exception of three paleolatitudes that are roughly concordant with present latitudes (Figure 8). Among the three exceptions, two of them are from Early Cretaceous volcanic rocks in the Mongolian belt [*Rozinov and Sholpo*, 1971; *Gorshkov et al.*, 1991]. A paleolatitude computed from the upper basalt series in the Tuoyun Basin of the southwest Tian Shan [*Meng et al.*, 1998] deviates far from values computed either for the same rock units in the basin [*Li et al.*, 1995; *Huang et al.*, 2005] or from the lower basalt series in the basin [*Li et al.*, 1995; *Meng et al.*, 1998; *Gilder et al.*, 2003]. The original authors explain this discrepancy in terms of a large displacement during the interval between eruption of the two basalt series. However, this claim has been refuted by the more recent studies on these basalt series [*Gilder et al.*, 2003; *Huang et al.*, 2005]. After discarding the above three paleolatitudes, we compare the remaining Paleogene and Cretaceous paleolatitudes with those predicted from the 60 and 120 Ma poles from stable Eurasia [*Besse and Courtillot*, 2002]. The standard deviations are 5.3 ± 7.1° and 6.3 ± 7.2° relative to the 120 and 60 Ma references, respectively, and indicate that the central Asian terranes are unlikely to have experienced northward movement on a scale discernible by paleomagnetism since onset of the India/Asia collision. The neotectonic northward convergence north of Tibet is therefore greatly less than the value of ~1500 km proposed from paleomagnetic results derived mainly from Cretaceous terrestrial sediments in the Tarim and Junggar regions of central Asia [*Chen et al.*, 1991, 1993]. Noting that most Cretaceous and Paleogene paleolatitudes are from the southwest Tian Shan with a location range of latitude 40–43°N and longitude 72–77°E (Table 3 and Figure 8); however, a conservative evaluation is that the southwest Tian Shan has possibly experienced a northward convergence of several hundred kilometers since onset of the India/Asia collision [*Dewey et al.*, 1989; *Avouac et al.*, 1993], but this is not discernible from paleomagnetism [e.g., *Bazhenov and Mikolaichuk*, 2002; *Gilder et al.*, 2003; *Huang et al.*, 2005].

7. Conclusions

[26] Geochronological and paleomagnetic study of the Halaqiaola basalts identifies extrusive magmatic activity in the Altai Mountains of northern Xinjiang at ~17 Ma and resolves no paleomagnetically discernible northward convergence north of the Altai Mountains since early Miocene times. The claim that Cenozoic magmatic activity is absent in the northern region of Xinjiang lying north to the Tian Shan Range is refuted. Paleomagnetic study of five Paleocene to Eocene red bed sites identifies ~20° of inclination flattening and highlights the major problem of using paleomagnetic data from red beds for resolving tectonic translation in central Asia. A new compilation of Cretaceous and Cenozoic paleomagnetic poles from volcanic rocks in central Asia further suggests that Neogene and Quaternary paleolatitudes deviate by 2.5 ± 7.4° to 2.8 ± 7.5° from the predicted values computed from the present-day latitude and from the 20 Ma paleopole for stable Eurasia, and indicate that no significant northward convergence has occurred north of Tibet since early Miocene times. The Cretaceous and Paleogene paleolatitudes are 5.3 ± 7.1° to 6.3 ± 7.2° south of the predicted values for interval between 120 and 60 Ma and still within the paleomagnetic confidence limits. It is therefore likely that central Asian terranes have experienced no more than a few hundred kilometers of neotectonic northward convergence since the time of the India/Eurasia collision. However, this view might be valid only in the southwest Tian Shan and more reliable data from elsewhere are required to rule out the possibility of post-collisional northward convergence in the other regions of central Asia.

[27] **Acknowledgments.** We are grateful to Yong'an Li, Dongjiang Sun, and Tao Liu for field assistance. This work was supported by the National Natural Science Foundation of China (grants 40525013, 40221402), the Ministry of Science and Technology of China (grant 2002CCA05100), and the Royal Society of UK at the form of KC Wong Education Foundation. Careful reviews by two anonymous reviewers improved the manuscript as did suggestions by the Associate Editor, Alexei Smirnov.

References

Achache, J., and V. Courtillot (1984), Paleogeographic and tectonics evolution of southern Tibet since middle Cretaceous time: New paleomagnetic data and synthesis, *J. Geophys. Res.*, *89*, 10,311–10,339.

Avouac, J. P., P. Tapponnier, M. X. Bai, H. Z. You, and G. Q. Wang (1993), Active thrusting and folding along the northern Tien Shan, and late Cenozoic rotation of the Tarim relative to Dzungaria and Kazakhstan, *J. Geophys. Res.*, *98*, 6755–6804.

Bazhenov, M. L., and A. V. Mikolaichuk (2002), Paleomagnetism of Paleogene basalts from the Tian Shan, Kyrgyzstan: Rigid Eurasia and dipole geomagnetic field, *Earth Planet. Sci. Lett.*, *195*, 155–166.

Besse, J., and V. Courtillot (2002), Apparent and true polar wander and the geometry of the geomagnetic field over the last 200 Myr, *J. Geophys. Res.*, *107*(B11), 2300, doi:10.1029/2000JB000050.

Besse, J., V. Courtillot, J. P. Pozzi, M. Westphal, and Y. X. Zhou (1984), Paleomagnetic estimates of Cenozoic convergence in the Himalayan thrusts and Zangbo suture, *Nature*, *311*, 621–626.

Bragin, V. Y., V. N. Reutsky, K. D. Litasov, V. G. Mal'kovets, A. V. Travin, and D. V. Mitrokhin (1999), Paleomagnetism and $^{39}Ar/^{40}Ar$ dating of Late Mesozoic volcanic pipes of Minusinsk Depression [Russia], *Phys. Chem. Earth, Part A*, *24*, 545–549.

Bureau of Geology and Mineral Resources of Xinjiang Uygur Autonomous Region (BGMRX) (1993), *Regional Geology of Xinjiang Uygur Autonomous Region*, *Geol. Mem. Ser.*, vol. 1, 841 pp., Geol. Publ. House, Beijing.

Buslova, M. M., T. Watanabe, Y. Fujiwara, K. Iwata, L. V. Smirnova, I. Y. Safonova, N. N. Semakov, and A. P. Kiryanova (2004), Late Paleozoic faults of the Altai region, central Asia: Tectonic pattern and model of formation, *J. Asian Earth Sci.*, *23*, 655–671.

Butler, R. F. (1992), *Paleomagnetism: Magnetic Domains to Geologic Terranes*, 238 pp., Blackwell, Malden, Mass.

Cande, S. C., and D. V. Kent (1995), Revised calibration of the geomagnetic polarity timescale for the Late Cretaceous and Cenozoic, *J. Geophys. Res.*, *100*, 6093–6095.

Chauvin, A., H. Perroud, and M. L. Bazhenov (1996), Anomalous low paleomagnetic inclinations from Oligocene–lower Miocene red beds of the south-west Tien Shan, Central Asia, *Geophys. J. Int.*, *126*, 303–313.

Chen, Y., et al. (1991), Paleomagnetic study of Mesozoic continental sediments along the northern Tien Shan (China) and heterogeneous strain in central Asia, *J. Geophys. Res.*, *96*, 4065–4082.

Chen, Y., J. P. Cogné, and V. Courtillot (1992), New Cretaceous paleomagnetic poles from the Tarim basin, northwestern China, *Earth Planet. Sci. Lett.*, *114*, 17–38.

Chen, Y., V. Courtillot, J. P. Cogné, J. Besse, Z. Y. Yang, and R. Enkin (1993), The configuration of Asia prior to the collision of India: Cretaceous paleomagnetic constraints, *J. Geophys. Res.*, *98*, 21,927–21,941.

Cogné, J. P., N. Halim, Y. Chen, and V. Courtillot (1999), Resolving the problem of shallow magnetizations of Tertiary age in Asia: Insights from paleomagnetic data from the Qiangtang, Kunlun, and Qaidam blocks (Tibet, China), and a new hypothesis, *J. Geophys. Res.*, *104*, 17,715–17,734.

Davydov, V. F., and A. Y. Kravchinsky (1971), Paleomagnetic directions and pole positions: Data for the USSR–Issue 1, in *Catalogue*, Sov. Geophys. Comm., World Data Cent. B, Moscow.

Day, R., M. Fuller, and V. A. Schmidt (1977), Hysteresis properties of titanomagnetites: Grain size and composition dependence, *Phys. Earth Planet. Inter.*, *13*, 260–267.

Dewey, J. F., R. M. Shackleton, C. Chang, and Y. Sun (1988), The tectonic evolution of the Tibetan Plateau, *Philos. Trans. R. Soc. London, Ser. A*, *327*, 379–413.

Dewey, J. F., S. Cande, and W. C. Pitman (1989), Tectonic evolution of the India-Eurasia collision zone, *Eclogae Geol. Helv.*, *82*, 717–734.

Dupont-Nivet, G., Z. Guo, R. F. Butler, and C. Jia (2002), Discordant paleomagnetic direction in Miocene rocks from the central Tarim Basin: Evidence for local deformation and inclination shallowing, *Earth Planet. Sci. Lett.*, *199*, 473–482.

Eroshkin, A. F. (1991), Paleomagnetism nizhnemelovih basaltov Svernoy Fergani, paper presented at IV All-Union Congress on Geomagnetism, Vladimir-Suzdal, Russia.

Fisher, R. A. (1953), Dispersion on a sphere, *Proc. R. Soc. London, Ser. A*, *217*, 295–305.

Gilder, S., Y. Chen, and S. Sen (2001), Oligo-Miocene magnetostratigraphy and rock magnetism of the Xishuigou section, Subei (Gansu Province, western China), and implications for shallow inclinations in central Asia, *J. Geophys. Res.*, *106*, 30,505–30,521.

Gilder, S., Y. Chen, J. P. Cogne, X. D. Tan, V. Courtillot, D. J. Sun, and Y. A. Li (2003), Paleomagnetism of Upper Jurassic to Lower Cretaceous volcanic and sedimentary rocks from the western Tarim Basin and implications for inclination shallowing and absolute dating of the M-0 (ISEA?) Chron, *Earth Planet. Sci. Lett.*, *206*, 587–600.

Goguitchaichvili, A., J. Morales, J. Urrutia-Fucugauchi, and A.-M. Soler (2001), On the use of continuous thermomagnetic curves in paleomagnetism: A cautionary note, *C. R. Acad. Sci. Earth Planet. Sci.*, *11*(333), 699–704.

Gorshkov, E. S., E. G. Gooskova, V. A. Starunov, T. S. Tyuleneva, Z. Ganhuyach, and P. Khosbayar (1991), Paleomagnitnie issledovaniya v zentralnoy Mongolii, paper presented at IV All-Union Congress on Geomagnetism, Vladimir-Suzdal, Russia.

He, H. Y., X. L. Wang, Z. H. Zhou, F. Wang, A. Boven, G. H. Shi, and R. X. Zhu (2004), Timing of the Jiufotang Formation (Jehol Group) in Liaoning, northeastern China and its implications, *Geophys. Res. Lett.*, *31*(12), L12605, doi:10.1029/2004GL019790.

Hrouda, F. (1982), Magnetic anisotropy of rocks and its application in geology and geophysics, *Geophys. Surv.*, *5*, 37–82.

Huang, B. C., Y. C. Wang, T. Liu, T. S. Yang, Y. A. Li, D. J. Sun, and R. X. Zhu (2004), Paleomagnetism of Miocene sediments from the Turfan Basin, northwest China: No significant vertical-axis rotation during Neotectonic compression within the Tian Shan Range, Central China, *Tectonophysics*, *384*(1–4), 1–21.

Huang, B. C., J. D. A. Piper, Y. C. Wang, H. Y. He, and R. X. Zhu (2005), Paleomagnetic and geochronological constraints on the post-collisional northward convergence of the southwest Tian Shan, NW China, *Tectonophysics*, *409*, 107–124.

Johnson, M. R. W. (2002), Shortening budgets and the role of continental subduction during the India–Asia collision, *Earth Sci. Rev.*, *59*, 101–123.

Kirschvink, J. L. (1980), The least-square line and plane and the analysis of paleomagnetic data, *Geophys. J. R. Astron. Soc.*, *62*, 699–712.

Krasa, D. (2002), Partial self-reversal of the NRM in basalts: Identifying the responsible mineral phases, *IRM Q.*, *12*(2), 3–4.

Le Pichon, X., M. Fournier, and J. Jolivet (1992), Kinematics, topography, shortening and extrusion in the India-Asia collision, *Tectonics*, *11*, 1085–1098.

Li, Y. A., Q. Li, H. Zhang, D. J. Sun, Y. D. Cao, and S. Z. Wu (1995), Paleomagnetic study of Tarim and its adjacent area as well as the formation and evolution of the basin, *Xinjiang Geol.*, *13*, 293–376.

McFadden, P. L. (1990), A new fold test for paleomagnetic studies, *Geophys. J. Int.*, *103*, 163–169.

Meng, Z. F., Y. S. Deng, T. H. Ding, C. P. Guang, Y. A. Li, and D. J. Sun (1998), Mesozoic-Cenozoic paleomagnetic results of volcanic rocks from the southern Tarim Basin, *Sci. China, Ser. D*, *28*, 79–89.

Merrill, R. T., and M. W. McElhinny (1983), *The Earth's Magnetic Field: Its History, Origin, and Planetary Perspective*, 401 pp., Elsevier, New York.

Meyer, B., P. Tapponnier, L. Bourjot, Y. Metivier, G. Gaudemer, S. K. Runcorn, G. Shunmin, and C. Zhitai (1998), Crustal thickening in Gansu-Qinghai, lithospheric mantle subduction, and oblique, strike-slip controlled growth of the Tibetan Plateau, *Geophys. J. Int.*, *135*, 1–48.

Molnar, P., and P. Tapponnier (1975), Cenozoic tectonics of Asia: Effects of continental collision, *Science*, *189*, 419–426.

Murphy, M. A., A. Yin, T. M. Harrison, S. B. Durr, Z. Chen, F. J. Ryerson, W. S. F. Kidd, X. Wang, and X. Zhou (1997), Did the Indo-Asian collision alone create the Tibetan Plateau?, *Geology*, *25*, 19–722.

Otofuji, Y., T. Itaya, H. C. Wang, and S. Nohda (1995), Palaeomagnetism and K–Ar dating of Pleistocene volcanic rocks along the Altyn Tagh Fault, northern border of Tibet, *Geophys. J. Int.*, *120*, 367–374.

Ozdemir, O., D. J. Dunlop, and B. M. Moskowitz (2002), Changes in remanence, coercivity and domain state at low temperature in magnetite, *Earth Planet. Sci. Lett.*, *194*, 343–358.

Patriat, P., and J. Achache (1984), India–Eurasia collision chronology has implications for crustal shortening and driving mechanisms of plates, *Nature*, *311*, 615–621.

Ren, S. M., R. X. Zhu, B. C. Huang, F. Q. Zhang, and H. Q. Wang (2004), Paleomagnetic study on orogenic belt: An example from Early Cretaceous volcanic rocks, Inner Mongolia, China, *Sci. China, Ser. D*, *47*(12), 1127–1133.

Renne, P. R., C. C. Swisher, A. L. Deino, A. B. Karner, T. L. Owens, and A. J. DePaolo (1998), Intercalibration of standards, absolute ages and uncertainties in $^{40}Ar/^{39}Ar$ dating, *Chem. Geol.*, *145*, 117–152.

Rozinov, M. I., and L. E. Sholpo (1971), Paleomagnetic directions and pole positions: Data for the USSR–Issue 1, in *Catalogue*, Sov. Geophys. Comm., World Data Cent.-B, Moscow.

Schult, A. (1968), Self-reversal of magnetization and chemical composition of titanomagnetites in basalts, *Earth Planet. Sci. Lett.*, *4*, 57–63.

Şengor, A. M. C., B. A. Natal'in, and V. S. Burtman (1993), Evolution of the Altaid tectonic collage and Phanerozoic crustal growth in Eurasia, *Nature*, *364*, 299–307.

Steiger, R. H., and E. Jäger (1977), Subcommission on geochronology: Convention on use of decay constants in geo- and cosmochronogy, *Earth Planet. Sci. Lett.*, *36*, 359–362.

Tan, X., K. P. Kodama, H. Chen, D. Fang, D. Sun, and Y. Li (2003), Paleomagnetism and magnetic anisotropy of Cretaceous red beds from the Tarim basin, northwest China: Evidence for a rock magnetic cause of anomalously shallow paleomagnetic inclinations from central Asia, *J. Geophys. Res.*, *108*(B2), 2107, doi:10.1029/2001JB001608.

Tapponnier, P., Z. Xu, F. Roger, B. Meyer, N. Arnaud, G. Wittlinger, and J. Yang (2001), Oblique stepwise rise and growth of the Tibetan Plateau, *Science*, *294*, 1671–1677.

Tauxe, L. (2005), Inclination flattening and the geocentric axial dipole hypothesis, *Earth Planet. Sci. Lett.*, *199*, 473–482.

Team of Regional Geological Survey of Xinjiang Uygur Autonomous Region (TRGSX) (1978a), Regional geological map of Qinghe County, scale 1:200,000, Geol. Publ. House, Beijing.

Team of Regional Geological Survey of Xinjiang Uygur Autonomous Region (TRGSX) (1978b), Regional geological map of Fuyun County, scale 1:200,000, Geol. Publ. House, Beijing.

Thomas, J. C., H. Perroud, P. R. Cobbold, M. L. Bazhenov, V. S. Burtman, A. Chauvin, and E. Sadybakasov (1993), A paleomagnetic study of Tertiary formations from the Kyrgyz Tien Shan and its tectonic implications, *J. Geophys. Res.*, *98*, 9571–9589.

Tong, Y. S., T. Qi, J. Ye, J. Meng, and D. F. Yan (1990), Tertiary stratigraphy of the north of Junggar Basin, Xinjiang (in Chinese with English abstract), *Vertebrata Palasiatica*, *28*(1), 59–90.

Wang, Q., et al. (2001), Present-day crustal deformation in China constrained by global positioning system measurements, *Science*, *294*, 574–577.

Xiao, X. C., Y. Q. Tang, Y. M. Feng, B. Q. Zhu, J. Y. Li, and M. Zhao (1992), *Tectonic Evolution of the Northern Xinjiang and Its Adjacent Region* (in Chinese with English abstract), Geol. Publ. House, Beijing.

Xingjiang Regional Stratigraphic Tables Compilation Team (XRSCT) (1981), *Regional Stratigraphic Tables of Northwestern China, Xinjiang Uygur Autonomous Region Volume*, 496 pp., Geol. Publ. House, Beijing.

Ye, J., W. Y. Wu, and J. Meng (2001a), Tertiary stratigraphy in the Ulungur River area of the northern Junggar Basin of Xinjiang (in Chinese with English abstract), *J. Stratigr.*, *25*(3), 193–200.

Ye, J., W. Y. Wu, and J. Meng (2001b), The age of Tertiary strata and mammal faunas in the Ulungur River area of Xinjiang (in Chinese with English abstract), *J. Stratigr.*, *25*(4), 283–287.

Yin, A., and T. M. Harrison (2000), Geologic evolution of the Himalayan-Tibetan Orogen, *Annu. Rev. Earth Planet. Sci.*, *28*, 211–280.

Zhang, Q. F., A. Q. Hu, G. X. Zhang, S. K. Fan, Z. P. Pu, and Q. X. Li (1994), Evidence from isotopic age for presence of Mesozoic and Cenozoic magmatic activities in Altai region, Xinjiang (in Chinese with English abstract), *Geochimica*, *23*(3), 269–280.

Zijderveld, J. D. A. (1967), A. C. demagnetization of rocks: Analysis of results, in *Methods on Paleomagnetism*, edited by D. W. Collinson et al., pp. 245–286, Elsevier, New York.

H. He, B. Huang, C. Zhang, and R. Zhu, Paleomagnetism and Geochronology Laboratory, Institute of Geology and Geophysics, Chinese Academy of Sciences, Beijing 100029, China. (bchuang@mail.iggcas.ac.cn)

J. D. A. Piper, Geomagnetism Laboratory, Department of Earth and Ocean Sciences, University of Liverpool, Liverpool L69 7ZE, UK.